RUPTURE MODEL OF THE TAURAMENA EARTHQUAKE (COLOMBIA JAN. 19/95)

N E PULIDO[1] And K IRIKURA[2]

SUMMARY

The Tauramena Earthquake occurred in Colombia in the eastern border of the North Andes, on the 19 of January of 1995 (ML=6.5), causing a considerable damage and several life losses. This paper summarizes the source rupture characteristics of that earthquake, obtained by performing a multitime window linear source inversion, using strong motion and teleseismic broadband data. The aftershock distribution of the earthquake shows two perpendicular fault planes, one corresponding to the mainshock, dipping to the northwest with a reverse fault mechanism, and the other corresponding to a big aftershock and dipping to the southeast. The slip distribution of the mainshock shows the existence of three asperities. The slip on the fault plane showed a strong change in orientation during the rupture specially for the region corresponding to the main asperities, suggesting a low level of initial shear stress. The final slip vector on the fault plane showed a large rotation in space, which could be explained by the presence of a strong barrier located besides the southern edge of the fault plane.

INTRODUCTION

The tectonics of the northern South America and Caribbean region is characterized by a complex interaction between the Nazca, Caribbean and South American plates.

The northern Andes (Andean block) is separated from the rest of South America by the Frontal Fault Zone (eastern border of the North Andes), and is moving N-NE with respect to the rest of South America and being compressed in an E-W direction [Pennington 1981, Kellog 1995]. The Frontal fault system consists of subparallel west-ward dipping faults, with a compressive principal stress oriented towards the fault, producing thrusting and right lateral slip [Freymueller et al. 1993, Taboada 1996].

The Tauramena earthquake was produced by the Frontal Fault, in particular the central segment of the Guaicaramo fault, which is a reverse fault with a general orientation of N40°E, and is dipping to the NW in a compressive stress regime [INGEOMINAS 1998].

The CMT solution of the mainshock shows a reverse mechanism, with almost no strike-slip component, which agrees with the tectonic conditions of the region. The general features of the earthquake are shown in Table 1 and Figure 1 (a).

Table 1. Source parameters of the Tauramena earthquake

Tauramena Earthquake	
Date	January 19/1995
Origin time (GMT)	15:05:05
Epicenter (INGEOMINAS)	5.01 N, -72.95W
Depth (CMT)	16 km
mb (CMT)	6.4
Strike (CMT)	212
Dip (CMT)	57
Rake (CMT)	87
Seismic Moment (CMT)	7.1E18 Nm

[1] *Disaster Prevention Research Institute, Kyoto University, Japan E-mail: nelson@egmdpri01.dpri.kyoto-u.ac.jp*
[2] *Disaster Prevention Research Institute, Kyoto University, Japan E-mail: nelson@egmdpri01.dpri.kyoto-u.ac.jp*

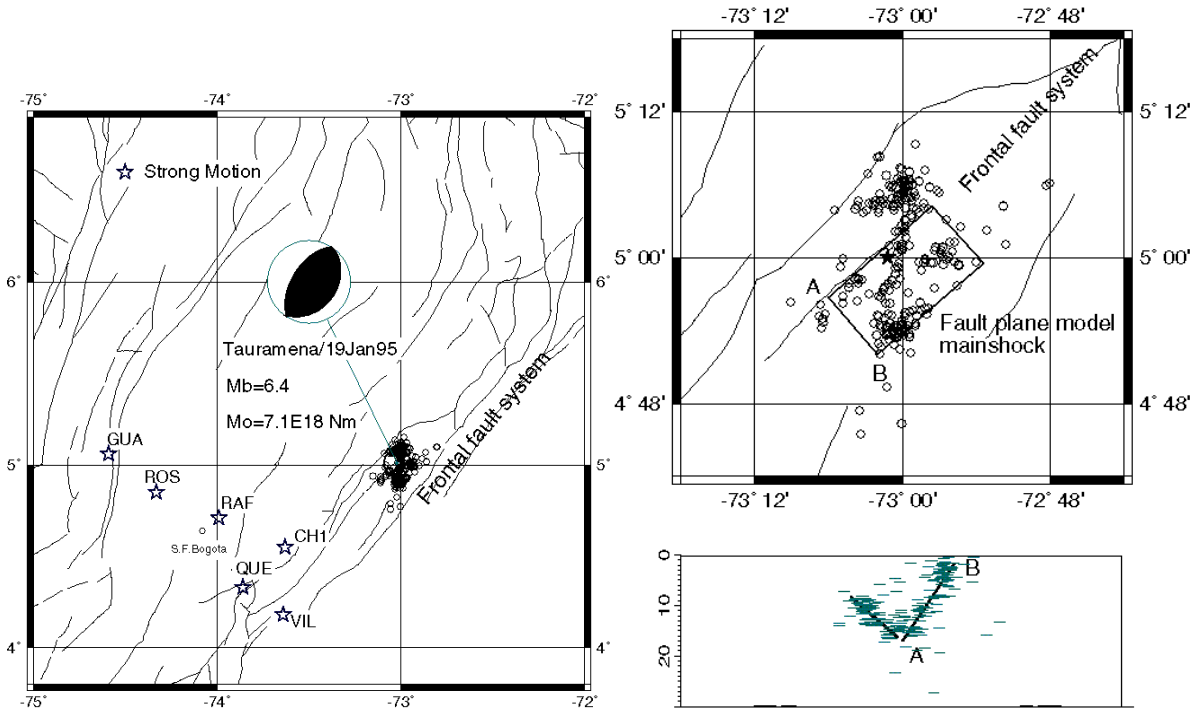

(a) (b)

Figure 1. (a) Strong Motion Stations used for the kinematic waveform inversion. (b) Aftershocks distribution of the Tauramena earthquake. The N40E cross section is shown. The mainshock fault plane model is corresponding to the segment AB. The star shows the location of the starting of the rupture.

FAULT RUPTURE MODEL

The Tauramena earthquake was modeled using a single fault segment with an area of 20 km x 20 km. The fault was discretized into 25 subfaults (4 km x 4 km). The ground motion at some particular station was calculated by summing up the seismograms generated by every subfault, represented by a point source, considering the corresponding time delay due to the rupture and propagation of the waves. The location, strike, dip and size of our model was assumed using the distribution of aftershocks obtained by a temporal network installed in the epicentral area [Dimate 1998].

According to the aftershock distribution, two fault planes with an approximate N50W direction could be identified. The first one dipping 50° to the NW and the second one perpendicular to the first and dipping 40° to the SE (figure 1b). The plane dipping to the NW is the one corresponding to the mainshock. As we can appreciate in Fig. 1b, the aftershocks corresponding to the mainshock are distributed mainly from 2 km to 20 km depth, which corresponds with the observation of no surface break. The complementary plane is corresponding to the aftershock distribution of a large aftershock that was triggered by the mainshock but is not belonging to the same event.

DATA

Strong Motion

The data we used for this work was recorded by the Colombian Strong Motion Network [INGEOMINAS 1995]. The strong motion data used was recorded by 12 bit accelerographs, with three components (SSA-2). From the available data set, we finally used six strong motion stations shown in table 2 and Figure 1a.

The displacement waveforms were used for the inversion, and all the data was bandpassed filtered from 0.1 to 1.0 hz. The displacement was obtained from the acceleration records by integrating them twice.

Table 2. Strong Motion and Short period Stations

Station	Location	N Lat.	W Long.	Site	Hipocentral distance
CH1	Chingaza	4.55	73.63	rock (tunnel)	94.6
VIL	Villavicencio	4.18	73.64	rock	122.5
RAF	San Rafael	4.71	73.99	rock (tunnel)	122.9
QUE	Quetame	4.33	73.86	rock	128.7
ROS	Rosal	4.85	74.33	rock	156.4
GUA	Guaduas	5.07	74.59	rock	184.1

Teleseismic data

For performing the inversion of the teleseismic data, we used broadband seismographs collected from the IRIS Global Seismic Network (16 stations), shown on Table 3. The stations selected have epicentral distances between 37° and 89°. The displacement waveforms were used and the data was bandpassed filtered from 0.002 to 1.0 Hz.

INVERSION METHOD

Inversion of Strong Motion data

A constrained, linear, least-squares inversion was used to calculate the slip at every element of the discretized fault, to give the best fit between the calculated and observed ground motions for all the stations, following the procedure by Hartzell & Heaton [1983]. The inversion was constrained in such a way that the slip is required to be non-negative and a smoothing condition is applied. Additionally we constrained the variation of the rake angle to 90° +/- 50°. We allow the multiple slip of every subfault by the use of a multi-time window procedure.

The inversion is an overdetermined system of linear equations as follow:

$$Ax \cong b \qquad (1)$$

where A is the matrix of the synthetics for all the subfaults (all components and time windows), x is the solution vector of slip weights, and b is the vector of observed ground motion.

The synthetics for the inversion of the strong motion and short period data, were calculated for each subfault for the strike-slip and dip-slip components. In total 500 seismograms were calculated for 10 components and 25 point sources, assuming a smoothed ramp function for the temporal variation of the slip.

The synthetics for the point sources were calculated using the Discrete Wave-Number methodology of Bouchon [1981] for a layered model, for frequencies up to 5 Hz.

The multiple time window procedure we used, consists of considering a source time function for every subfault, resulting from the time-delayed summation of 5 smoothed ramp functions with a rise time of 1 sec. In this way we allow the inversion to adjust the slip and rise time for every subfault up to a value of 3 sec. A rupture velocity of 2.7 km/sec was used. Since the depth of the earthquake is not well constrained, several runs were done for different starting points of the rupture.

Velocity Structure

The velocity structure model used to calculate the synthetics is shown in Table 4. The model was basically obtained from the aftershock arrival times recorded by the temporal network, by performing a simultaneous inversion for the velocity structure and the location of the aftershocks [Dimate 1998]. The model was adjusted for every station, by matching the observed P and S arrivals of several aftershocks, with the corresponding simulated seismograms.

Table 3. List of parameters of Teleseismic Stations

Station	Azimuth angle	Back Azimuth Angle	Distance (degree)
HRV	1.6	-177.9	37.2
KEV	19.9	-79.0	88.6
KONO	30.4	-93.9	81.8
DSB	35.2	-106.2	71.9
DPC	39.8	-87.3	85.5
PAB	49.7	-100.0	70.2
GRFO	40.5	-91.2	82.3
RAR	-111.4	84.1	89.0
PAS	-49.3	114.2	50.9
TUC	-47.7	119.3	44.5
CMB	-45.8	115.1	54.1
COR	-39.8	116.4	59.0
NEW	-33.6	124.2	57.1
COL	-24.7	101.5	79.0
BINY	-3.8	174.8	37.0
PMSA	176.0	-9.3	70.1

Table 4. Velocity model for the Tauramena earthquake

Depth (km)	Vp (km/sec)	Vs (km/sec)	ρ (g/cm^3)	Qs	Qp
0-3	4.69	2.69	2.0	200	100
3-6	4.92	2.83	2.3	350	175
6-9	5.29	3.04	2.5	400	200
9-15	5.57	3.20	2.6	500	250
15-24	6.23	3.58	2.7	600	300
>24	7.00	4.02	2.9	900	450

Inversion of Teleseismic data

In order to check the validity of the model obtained by the inversion using strong motion and short period data, we also performed the source inversion using teleseismic body waves.

P-wave records (vertical components) were inverted by means of the iterative deconvolution method [Kikuchi & Kanamori, 1982, 1991]. The Tauramena earthquake was modeled by a multiple event sequence.

INVERSION RESULTS

Rupture process from the Strong Motion data

Since the hypocenter of the mainshock is not well constrained, several runs for different locations of the starting point were considered. The model who gave the best waveform fitting, was the one with the location of the rupture initiation at the bottom of the fault (the open circle in Fig. 2b). The slip distribution obtained is shown in Figure 2. The viewpoint is from the footwall of the fault (SE-NW). From that figure we can observe the existence of three asperities; the first one located in the north-east bottom corner of the fault at a depth of approximately 17 km, the second one located at the center of the south-west edge of the fault at a depth of 8 km, and the third one in the upper NE corner at a depth of 3.5 km. We can also observe that the total duration of the moment release is around 10 sec (Fig.2a).

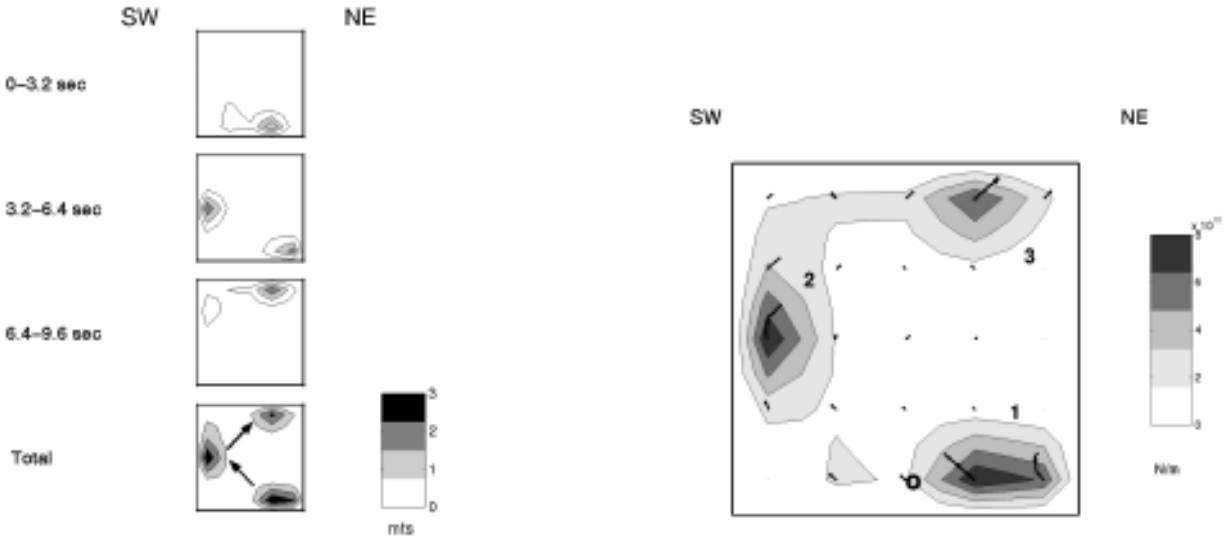

(a) (b)

Figure 2. (a) Time progression of the rupture and final slip distribution of the Tauramena earthquake. (b) Total moment release over the fault plane and temporal variation of the slip vector for the 5 time windows.

The rupture started from the center bottom of the fault, very close to the asperity N° 1, then propagated upwards to the SW (asperity N°2) and experienced a strong rotation to the NE to finally break the asperity N°3. The rupture sequence is shown by the arrows in Fig. 2a. The strong rotation of the slip in the region around the asperity N°2 could be explained by the presence of a strong barrier located to the south of the SW edge of the fault. In fact the seismo-tectonic characteristics of the region show that in the area immediately south of the rupture of the earthquake, there is an anomalously low seismicity zone, compared with the base seismicity of the frontal fault, which may correspond to a seismic gap (INGEOMINAS 1998).
Besides the spatial rotation of the slip, a strong rotation of the slip during the rupture could be observed for the asperities 1 and 2. That rotation can be appreciated in figure 2b, where we show with arrows at every subfault the path described by the slip vector for the five consecutive time windows. This feature suggests a low initial stress and a spatial variation of the slip orientation [Guatteri and Spudich, 1998]

Inversion of Teleseismic data

In order to confirm the validity of the three asperities model obtained with the strong motion, we analyzed two models with the teleseismic data. The first one consists of a moment tensor inversion of a single point source. The solution shows a good fitting of the waveforms as can be seen on Fig. 3a.

The second model consists of three point sources, corresponding to the three asperities obtained previously. Several runs were done varying the depth and rupture sequence of the three asperities as initial models of the teleseismic inversion. Finally the best model obtained, was the one corresponding to a rupture time sequence similar to the one obtained with the strong motion data (Fig. 4). The waveform fitting of the three asperities model is improved with respect to the single asperity model (Fig. 3a). In Figure 3 we can appreciate a change in slope for all the observed waveforms (upper trace) around 10 sec. We believe that this feature which could not be reproduced by the single point source model, was produced by the asperity N°3 located in the upper part of the fault plane and breaking at approximately 8 sec (Fig. 4).
The teleseismic inversion confirms the existance of three asperities in the fault plane, as in the strong motion case, however the contribution of the asperity N° 2 is not so significant in the teleseismic waveforms.

CONCLUSIONS

-The distribution of aftershocks shows the presence of two perpendicular faults, the one dipping to the west corresponding to the mainshock.
-The slip distribution obtained from the strong motion data shows the existence of three asperities in the fault plane.

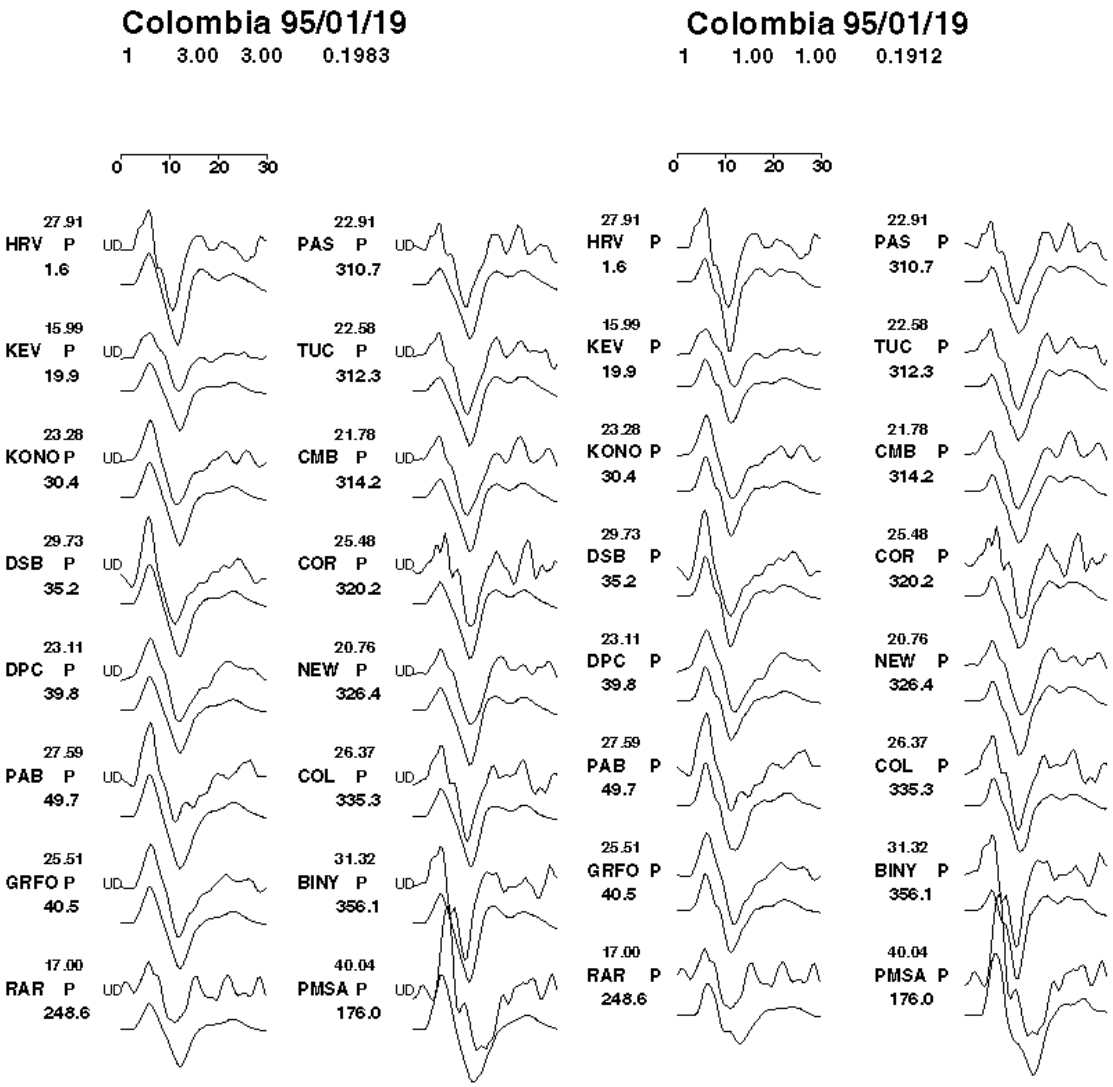

Figure 3. (a) Comparison of the observed (upper) and calculated teleseismic P-waveforms (lower), for one point source model of the Tauramena earthquake. The observed maximum amplitude, station name and azimuth are also shown. (b) Same comparison for the three asperities model.

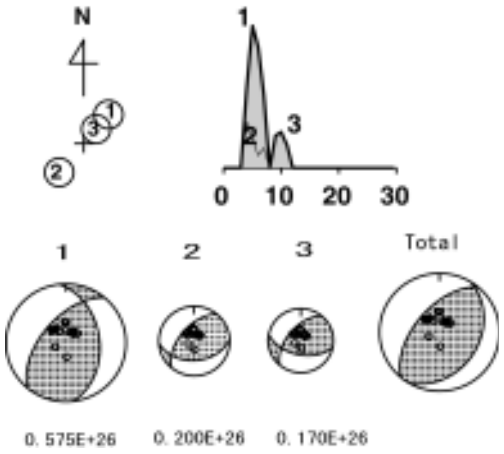

Figure 4. Source time function, focal mechanism and seismic moment of the two three sources model of the Tauramena earthquake (dyne. cm).

-The slip showed a very strong spatial rotation in the fault plane which could be explained by the a heterogeneous distribution of the initial stress and the presence of a barrier close to the southern edge of the fault.
-A rotation of the slip during the rupture was also observed, which suggest a spatial variation of the slip and a low level of initial shear stress.
-The simulation of the strong motion can benefit in great manner from the studies of the source (kinematics inversions), because the source process is very complex, and its oversimplification could lead to a under or overestimation of the ground motion.

REFERENCES

Bouchon, M. (1981). "A simple method to calculate Green's functions for elastic layered media" , *Bull. Seism. Soc. Am.* 71, 959-971.

Dimate, C. (1998). "Aftershock sequence of the Tauramena earthquake", INGEOMINAS, Report project A98F02, INGEOMINAS (in Spanish).

Freymueller, J. T., J. N. Kellogg & V. Vega (1993). "Plate motions in the North Andean region", *J. Geophys. Res.,*98 (B12), 21,853-21,893.

Guatteri M. & P. Spudich (1998). "Coseismic temporal changes of slip direction: The effect of absolute stress on dynamic rupture", *Bull. Seism. Soc. Am.* 88, 777-789.

Hartzell, S. H. & T. H. Heaton (1983). "Inversion of strong motion and teleseismic waveform data for the fault rupture history of the 1979 Imperial Valley, California, earthquake", *Bull. Seism. Soc. Am.* 73, 1553-1583.

INGEOMINAS (1995). *Boletin trimestral de sismos,* Vol. 3 N°1, *Boletin de movimiento fuerte,* Vol. 1 N°1.

INGEOMINAS (1998). "Seismotectonics of the Eastern Andean margin", Report project A98F02, INGEOMINAS (in Spanish).

Kellogg, J & V. Vega (1995). "Tectonic development of Panama, Costa Rica, and the Colombian Andes: Constraints from Global Positioning System geodetic studies and gravity", *Geol. Soc. Am*., Special Paper 295, 75-90

Kikuchi, M. & H. Kanamori (1982). "Inversion of complex body waves", *Bull. Seism. Soc. Am.* 72, 491-506.

Kikuchi, M. & H. Kanamori (1991). "Inversion
of complex body waves III", *Bull. Seism. Soc. Am* 81, 2335-2350.

Mendoza, C & S. H. Hartzell (1988). "Aftershocks patterns and mainshock faulting", *Bull. Seism. Soc. Am.* 78, 1438-1449.

Pennington W. D. (1981). "Subduction of the eastern Panama basin and seismotectonics of northwestern South America", *J. Geophys. Res.,*86 (B11), 10,753-10,770.

Taboada A. (1996). Estudios tectónicos y neotectónicos, proyecto microzonificación sismica de Santafé de Bogotá", INGEOMINAS, Universidad de los Andes.